26

Deep Hydrocarbon Cycle: An Experimental Simulation

Vladimir Kutcherov[1,2], Kirill Ivanov[3], Elena Mukhina[4], and Aleksandr Serovaiskii[2]

ABSTRACT

The concept of a deep hydrocarbon cycle is proposed based on results of experimental modeling of the transformation of hydrocarbons under extreme thermobaric conditions. Hydrocarbons immersed in the subducting slab generally maintain stability to a depth of 50 km. With deeper immersion, the integrity of the traps is disrupted and the hydrocarbon fluid contacts the surrounding ferrous minerals, forming a mixture of iron hydride and iron carbide. This iron carbide transported into the asthenosphere by convective flows can react with hydrogen or water and form an aqueous hydrocarbon fluid that can migrate through deep faults into the Earth's crust and form multilayer oil and gas deposits. Other carbon donors in addition to iron carbide from the subducting slab exist in the asthenosphere. These donors can serve as a source of deep hydrocarbons that participate in the deep hydrocarbon cycle, as well as an additional feed for the general upward flow of the water-hydrocarbon fluid. Geological data on the presence of hydrocarbons in ultrabasites squeezed from a slab indicate that complex hydrocarbon systems may exist in a slab at considerable depths. This confirms our experimental results, indicating the stability of hydrocarbons to a depth of 50 km.

26.1. INTRODUCTION

Descriptions of the global carbon cycle are generally limited to processes occurring in the oceans, the atmosphere, and in the surface sedimentary layer of the Earth's crust. Knowledge of the deep carbon cycle is fragmentary, despite the fact that the deep layers of the Earth may contain up to 90% of all planetary carbon (Javoy, 1997). It is assumed that the upward flux of carbon is formed mainly from CO_2 and CH_4 during volcanic eruptions and the downward flow is realized in subduction zones (Manning, 2014). Subduction processes play a key role in the evolution of the continental crust and upper mantle (Dasgupta et al., 2013; Stern, 2002).

Despite the significant progress in understanding the processes of subduction, the potential role of hydrocarbons in subduction zones is not well understood and has long been debated (Manning, 2004). Numerous major petroleum deposits have been located close to subduction zones (Hessler & Sharman, 2018; Mann et al., 2003). Hydrocarbons located in these zones sink with the subducting slab while being exposed to extremely high temperatures and pressures. Taking into consideration the ~44,500 km length of global subduction zones, Kelemen and Manning (2015) suggest that the total amount of immersed hydrocarbons is likely significant.

[1] *KTH Royal Institute of Technology, Stockholm, Sweden*
[2] *Gubkin University, Moscow, Russia*
[3] *The Zavaritsky Institute of Geology and Geochemistry, Ekaterinburg, Russia*
[4] *Skolkovo Institute of Science and Technology, Moscow, Russia*

Carbon in Earth's Interior, Geophysical Monograph 249, First Edition. Edited by Craig E. Manning, Jung-Fu Lin, and Wendy L. Mao.
© 2020 American Geophysical Union. Published 2020 by John Wiley & Sons, Inc.

Furthermore, hydrocarbons in the ocean crust sinking with the subducting slab could have been generated inside the slab at a comparably shallow depth. The experimental results presented in Mukhina et al. (2017) demonstrated that the formation of complex hydrocarbon mixtures can occur at a depth of 70–80 km in the subducting slabs. Petrological observation and experimental simulation also confirmed that carbonates and water sinking with the subducting slab are transformed into graphite and light saturated hydrocarbons (Tao et al., 2018). Estimations of the carbon content of subduction-zone fluids show that organic carbon species may also be present in the deep Earth (Sverjensky et al., 2014).

The abiogenic formation of complex hydrocarbon systems in the upper and lower mantle and their upward migration to the Earth's crust was investigated in a series of studies (Belonoshko et al., 2015; Kenney et al., 2002; Kolesnikov et al., 2009; Kutcherov et al., 2010; Sokol et al., 2017; Sonin et al., 2014). Although Kolesnikov et al. (2017) conducted a thorough review of theoretical and experimental studies on the possible pathways for the formation of complex hydrocarbons at pressures and temperatures of the upper mantle, the behavior of hydrocarbons in subducting slabs is still not well understood.

In the subduction zone, at a depth of 50–80 km, the temperature at the boundary of the plates coincides with the continental geotherm and reaches 600°–700 °C (Karato, 2013). If pressure increases to 0.5–1 GPa, the melting temperature for the majority of silicates in the presence of water drops to 600°–700 °C (Bezmen et al., 2005; Shimada, 1969). Water-saturated carbonates, the predominant carbon-bearing phases commonly present in the subducting slab, behave similarly (Cooper et al., 1975). Concurrently, alumosilicates and water-saturated carbonates also melt at depths of 50–80 km. Thus, we suggest that hydrocarbon traps retain their integrity at depths of 50–80 km. With further immersion, the integrity of the traps is disrupted and the hydrocarbon fluid begins to contact the surrounding iron-bearing minerals.

26.2. MATERIALS AND METHODS

Two different types of high-pressure equipment, described below, were employed: diamond anvil cells and the Toroid-type large reactive volume unit.

26.2.1. Diamond Anvil Cells

Diamond anvil cells with a culet diameter of 250 μm were used with steel or rhenium gaskets (250 μm thickness) with the 125 μm hole drilled in the center. The hole was filled with the liquid hydrocarbon system that also served as a pressure medium in the experiments. Cell temperature and pressure were measured by the fluorescence of the ruby (Cr-doped Al_2O_3) and Sm:YAG (Sm-doped $Y_3Al_5O_{12}$) chips loaded into the chamber together with the sample (Mao et al., 1986; Trots et al., 2013). Two different heating methods were applied in the experiments: resistive and laser heating.

The resistive heating method was used for the experiments with temperatures up to 450 °C, carried out by a Pt heater installed inside the body of the cell. The temperature was measured by the ruby fluorescence. A Pt/Pt-Rh (10%) thermocouple was mounted on the side surface of the diamond for additional temperature control during heating. Prior to heating, the sample was loaded into the chamber and the cell was closed and pressurized using the screws on the body of the cell. The temperature was increased at a rate of 50°–60 °C per hour, according to the thermocouple readings. The temperature and pressure inside the cell were monitored two to three times per hour by measuring the fluorescence of ruby and Sm:YAG. The pressure was kept constant during the heating. After the required temperature was reached, the cell was kept at the required thermobaric parameters for several hours. Then the heating was stopped and the sample was quenched. The sample analysis was carried out by means of the Raman spectrometer LabRam coupled with the He-Ne laser (514.5 nm wavelength and the power 0.001–0.6 W).

In the laser heating experiments, the systems, consisting of a mixture of saturated hydrocarbons C_{15}-C_{40} (99.9%, Merch KGaA, EMD Millipore Chemical 1.07160.1000) and ^{57}Fe-enriched wüstite $Fe_{0.94}O$ (in the first series) and pyroxene-like glass $(Mg_{0.91}Fe_{0.09})(Si_{0.91}Al_{0.09})O_3$ (in the second series), were heated by the portable laser heating setup, with two optical fibre-based opposite-mounted 50 and 100 W (900°–1500 °C) power lasers (Kupenko et al., 2012). The temperature of the heated surface of the sample was measured by means of multiwavelength spectroradiometry of the sample radiation (Dubrovinsky & Saxena, 1999). The temperature radiation spectra were collected in the wavelength range of visible light and near infrared light (600–900 nm); afterwards, the spectra were fitted by means of the Planck function. The heating experiment continued for 5 minutes with constant movement of the focal point of the laser for equal heating of the surface of the sample. The analysis was carried out by means of conventional Mössbauer spectroscopy (with the source ^{57}Co) and Raman spectroscopy at experimental pressure and ambient temperature before and after heating. The isomer shift and the velocity

scale were calibrated relative to α-Fe. The transmission Mössbauer spectra were fitted to Lorentzian line-shapes by MossA software (Prescher et al., 2012).

26.2.2. The Toroid-Type Large Reactive Volume Unit

The Toroid-type large reactive volume unit enabled the investigation of sample transformation at pressures up to 8 GPa and temperatures up to 1800 K with the time exposure of the required conditions from one second up to several days. An experimental assemblage included a couple of hard-alloy anvils, also known as anvils-with-hole, one toroid-type chamber, one cylindrical sample container, and two graphitic resistive heaters. The hydraulic pressure applied to pistons of the device was transferred to the anvils and, finally, to the sample container. The Toroid-type chamber served as a pressure medium, transmitting the pressure equally to the surface of the sample container. One of the main advantages of the Toroid-type chamber is the possibility of using large-volume containers, up to 0.3 cm^3, that enable ex situ chromatography analysis to be carried out.

The mixture of water and iron carbide (Fe_3C, American Elements, CAS# 12011-67-5) was loaded into a sealed steel container and then placed inside the Toroid-type chamber. Water was loaded in excess amount to reach the full transformation of iron carbide. Two resistive heaters (made of the mixture graphite-Al_2O_3) were placed above and below the container. Then the sample assemblage was placed between two hard-alloy anvils. Pressurizing the carefully calibrated internal and external diameters of the cylindrical container produced a sealed zone inside the container. Water served as a pressure medium for the container, preventing it from being crushed.

When experimental pressure was reached, the heating was turned on. All the variables (the hydraulic pressure, electrical power, duration of the exposure, and further quenching) were adjusted using the press control software. The temperature and pressure in the container were measured using calibration curves, made for particular containers, chambers, and samples by phase transitions of reference compounds (Bi, PbSe, PbTe for pressure calibration, Pb, Sn, Ti, Cu for temperature calibration). After the sample was exposed for a certain time, the heating was switched off and the sample was quenched. Once the temperature had dropped to ambient, the container was depressurized and recovered from the chamber. The pressure-sealed steel container maintained chemical product integrity. The products were analyzed by means of gas chromatography.

A "Chromatek 5000" gas chromatograph was used for analysis thanks to a specific gas-extracting device. The sealed gas-extracting cell was used to remove the gaseous product from the container by going down a sharp steel stock, making a hole in the container and recovering the products. Helium as carrier gas was supplied from the system of the chromatograph, taking the gaseous product to the chromatograph. The chromatograph was equipped with a capillary column and two flame ionisation detectors. This analytical equipment enabled light hydrocarbons and inorganic gases to be detected and measured. The details of the experimental method are described in Mukhina et al. (2017). Following chromatography analysis, the solid products were recovered from the steel container and analyzed by powder X-ray diffraction. A Seifert MZ III powder X-ray diffractometer, employing CuK_α radiation (1.5405981 Å) in the Bragg-Brentano geometry, was used.

26.3. EXPERIMENTAL RESULTS

The results of three series of experimental investigation are presented below. Each experiment in each series was repeated three times to confirm results.

26.3.1. Behavior of the Hydrocarbon Systems at Depths Down to 50 km

In the first series of the investigation, the model hydrocarbon system, similar to natural gas condensate, was used (density ρ_{20}^4 794.7 kg/m^3; Table 26.1). The experiments were carried out in diamond anvil cells with resistive heating at temperatures of 320°–450 °C and pressures of 0.7–1.4 GPa with various exposure times (Table 26.2). Raman spectroscopy was employed for product analysis. The experimental results demonstrated the thermal stability of the hydrocarbon system at the thermobaric conditions applied. The example of the Raman spectra of the model hydrocarbon system (before and after heating at 450 °C and 1.4 GPa) is presented in Figure 26.1.

The composition of the hydrocarbon system remained constant in all three experiments of the current series of the investigation. All peaks of the spectra, corresponding to hydrocarbons of the model system, kept their relative intensity, shape, and Raman wavelength shift. No new peaks appeared in the spectra after heating, signifying the absence of new components in the sample. Increasing exposure time from 3 to 12 hours did not influence the composition of the hydrocarbon system (Experiment 3, Table 26.2).

The results of the first series of the experimental investigation demonstrated that the hydrocarbon system,

Table 26.1 Characteristics of the model hydrocarbon system.

Compound	Content, %
Aromatics	55
Paraffins	40
Naphthenes	5
Asphaltenes	0
Sulphur	0

Table 26.2 Conditions of the experiments with model hydrocarbon system.

Exp.	Pressure, (±0.2) GPa	Temperature, (±20) °C	Corresponding depth, km	Exposure time, hours
1	0.7	320	20–30	3
2	1.2	420	30–40	3
3	1.4	450	40–50	12

similar to natural gas condensate, retained its qualitative and quantitative composition in the thermobaric range 320°–450 °C and 0.7–1.4 GPa, corresponding to a depth down to 50 km.

26.3.2. Hydrocarbon System Transformation at a Subduction Depth Down to 290 km

In the second series of the experimental investigation, the behaviour of the system, consisting of a mixture of saturated hydrocarbons C_{15}-C_{40} and iron-bearing minerals, was investigated. As iron-bearing minerals, ^{57}Fe-enriched pyroxene-like glass $(Mg_{0.91}Fe_{0.09})(Si_{0.91}Al_{0.09})O_3$ and wüstite $Fe_{0.94}O$ composition, synthesized by Kantor et al. (2004), were used. The powder of ^{57}Fe-enriched pyroxene-like glass was synthesised from a pelletized mixture of Fe_2O_3, $Mg(OH)_2$, SiO_2 and $Al(OH)_3$ using a 1 atmosphere box furnace. Two experiments were carried out in diamond anvil cells with the laser heating in this series (Table 26.3).

The Mössbauer spectra of the samples, collected before and after heating, show a mixture of iron hydride FeH (Narygina et al., 2011) and iron carbide Fe_7C_3 (Prescher et al., 2015) (with trace amount of α-Fe and an unidentified iron compound) detected in both experiments as a result of the chemical interaction between the hydrocarbon system and the iron-bearing minerals (Figure 26.2). Raman spectroscopy analysis demonstrated the formation of graphite (Tuinstra & Koenig, 1970), water in the form of ice VII (Walrafen et al., 1982), and methane (Kolesnikov et al., 2009; Sterin et al., 2013) (Figure 26.3). Pure hydrogen was not detected in the sample after the heating.

According to the experimental results obtained, the chemical reaction may be described as follows:

$$7.5\,\text{GPa}: \text{FeO}(\text{wüstite}) + C_nH_{2n+2} \rightarrow \text{FeH} + Fe_7C_3 + C + H_2O + CH_4 \quad (26.1)$$

$$8.8\,\text{GPa}: \text{FeSiO}_3\,(\text{in the form of pyroxene}) + C_nH_{2n+2} \rightarrow \text{FeH} + Fe_7C_3 + C + H_2O + CH_4 \quad (26.2)$$

Summarizing our observations, we conclude that heating of hydrocarbons with iron oxides or silicates to temperatures above 1000 °C and pressures above 7 GPa results in

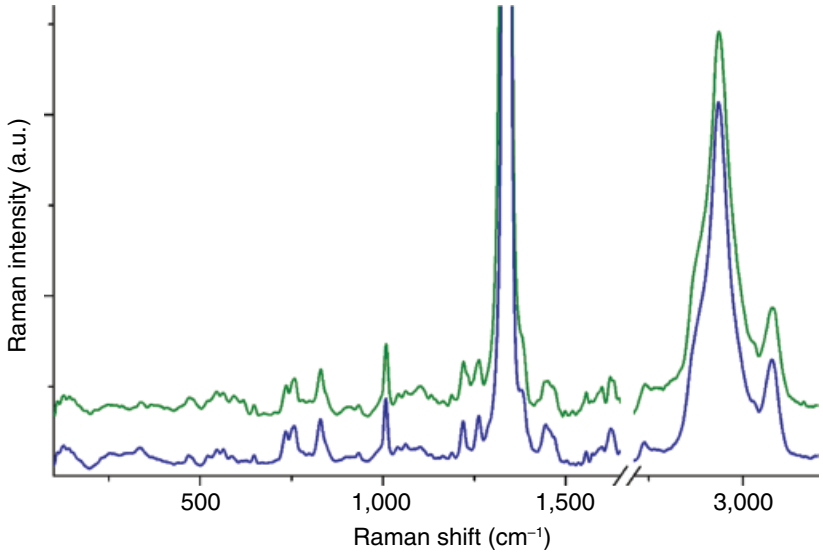

Figure 26.1 The Raman spectra of the model hydrocarbon system at 1.4 GPa before heating (blue curve) and after 12 hours of heating at 450 °C (green curve). See electronic version for color representation of the figures in this book.

Table 26.3 Experimental details.

Exp #	System	Final P, (±0.2)GPa	T, (±100) °C	Mössbauer Spectroscopy Results	Raman Results
1	Paraffin oil + wüstite $Fe_{0.94}O$	7.5	1100	FeH + Fe_7C_3	C + H_2O + CH_4
2	Paraffin oil + pyroxene-like glass $(Mg_{0.91}Fe_{0.09})(Si_{0.91}Al_{0.09})O_3$	8.8	1300	FeH + Fe_7C_3 + remaining pyroxene glass	C + H_2O + CH_4

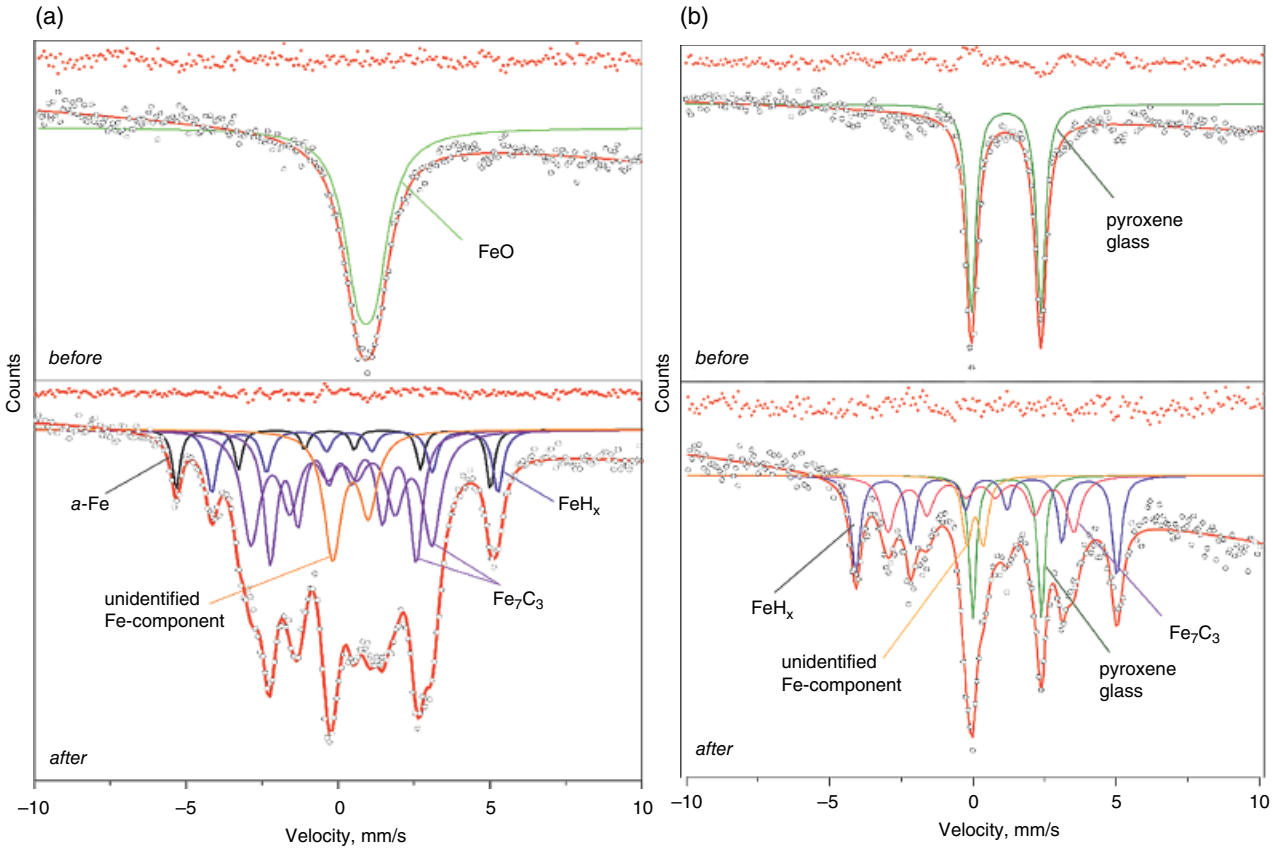

Figure 26.2 The Mössbauer spectra of the samples: (a) At 7.5 GPa before heating: doublet of $Fe_{0.94}O$ with a narrow quadrupole splitting; after laser heating: produced Fe_xH (blue sextet), Fe_7C_3 (two purple doublets), α-Fe (black sextet), and an undefined iron component. (b) At 8.8 GPa before heating: doublet of pyroxene glass; after heating: produced Fe_xH (blue sextet), Fe_7C_3 (purple doublet), remained pyroxene glass and an undefined iron component. See electronic version for color representation of the figures in this book.

formation of a mixture of iron hydride and iron carbide in the subducting slab. It is notable that formation of this mixture was observed independently of whether iron-bearing silicate or oxides were used as starting materials.

The ability of iron carbide to act as a carbon donor in the deep abiogenic synthesis of hydrocarbon systems was investigated on the third series of experiments.

26.3.3. Chemical Interaction of Iron Carbide and Water at the Thermobaric Conditions of the Asthenosphere

In the third series of the current experimental investigation, the chemical reaction between iron carbide (Fe_3C) and water was studied in the thermobaric range, corresponding to depths of 100–150 km. Two experiments were carried out: the first one at 3.5 GPa and 750 °C, and the second one at 4.5 GPa and 850 °C. The experiments were carried out in the Toroid-type large reactive volume unit. The gas chromatograph "Chromatech-5000" was employed for the reaction products analysis with the further analysis of solid products by powder X-ray diffraction data. The X-ray diffraction analysis demonstrated full transformation of iron carbide (the distinguishable peaks of Fe_3C were absent on the spectra after the heating; Kumari et al., 2016; Williams et al., 2016) with the formation of wustite FeO (Khurshid et al., 2013) (Figure 26.4). The results of the experiments demonstrated the chemical interaction

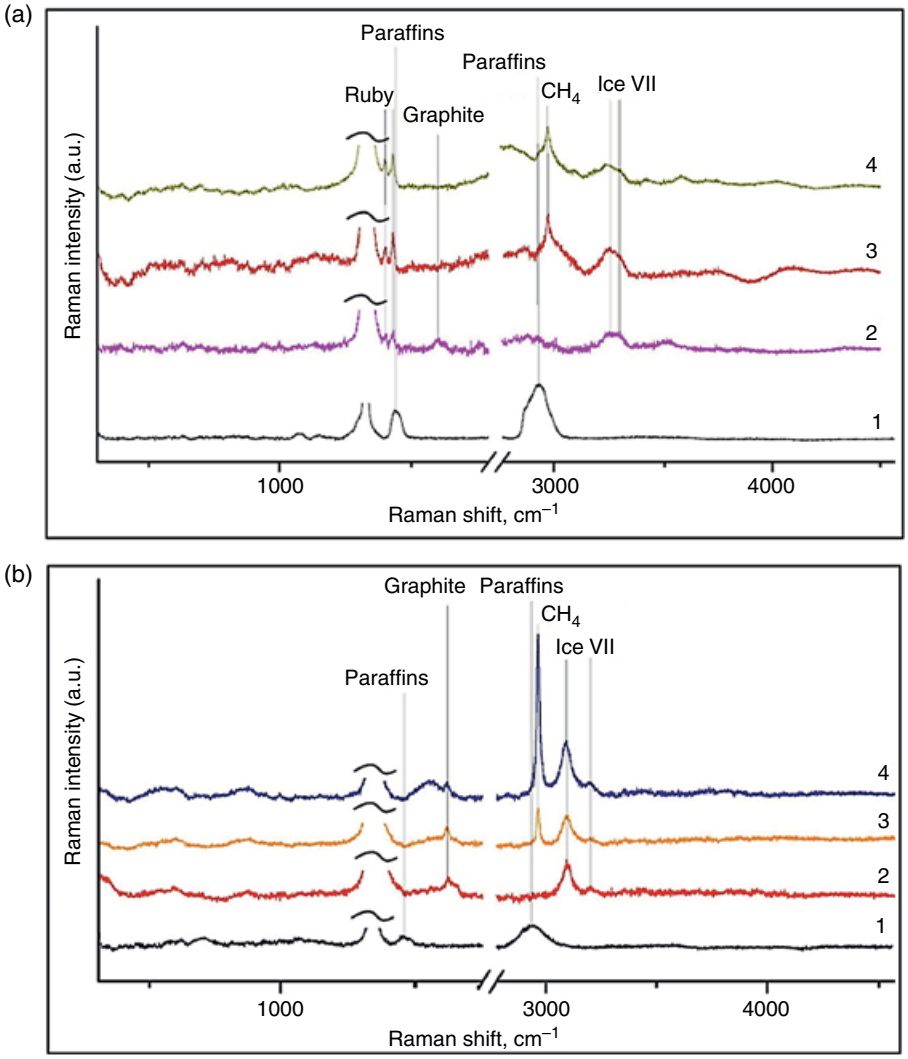

Figure 26.3 The Raman spectra of the sample before and after laser heating at 7.5 GPa (a) and 8.8 GPa (b). Number on the spectra: 1 = before heating; 2–4 = after heating, from the less heated zone on the border of DAC (2) to the more heated zone in the center of DAC (3, 4). See electronic version for color representation of the figures in this book.

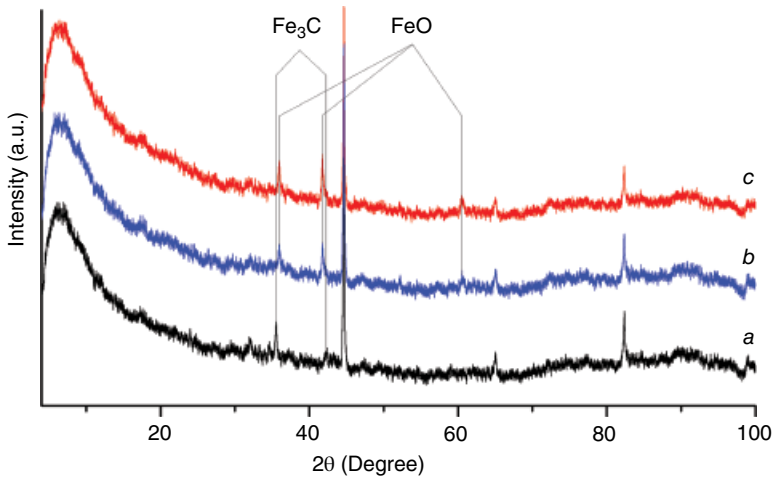

Figure 26.4 XRD pattern of pure iron carbide Fe_3C (a), solid products of the chemical reaction between Fe_3C and H_2O at 750 °C and 3.5 GPa (b), solid products of the chemical reaction between Fe_3C and H_2O at 850 °C and 4.5 GPa (c). See electronic version for color representation of the figures in this book.

between iron carbide and water under the above-mentioned thermobaric conditions with the formation of complex hydrocarbon mixtures, consisting of light paraffins and naphtenes (Figure 26.5). As can be seen in Figure 26.5, the formation of heavier hydrocarbons is prevalent at lower thermobaric conditions, corresponding to upper levels of the mantle. According to the experimental results, the chemical reaction proceeded according to the following scheme:

$$Fe_3C + H_2O \rightarrow FeO + C_nH_{2n+2} + C_mH_{2m} \quad (26.3)$$

The thermobaric conditions for all the experiments discussed above are shown in Figure 26.6, which also presents pressure-temperature profiles of the coldest and hottest subducting slabs and Earth's geotherm.

26.4. GEOLOGICAL OBSERVATIONS

Our experimental results demonstrate that hydrocarbons in the slab maintain their stability to a depth of 50 km. In this study, we compared the experimental results with geological observations from a well-studied ancient island-arc system, the Urals. Signs of subduction are clearly manifested in the Urals. Signs of subduction are clearly manifested in the Urals. The Main Uralian Fault (MUF) is the paleozone of subduction (K. Ivanov, 2001). It extends in the sub-meridional direction for more than 2000 km and divides the Urals fold belt into two sectors, the western (paleocontinental) and the eastern (paleoisland-arc). Here, the oceanic plate of the Early Paleozoic Ural Paleoocean sinks under the Irendyk island arc (Zonenshain et al., 1991). Structural and paleomagnetic data indicate that subduction

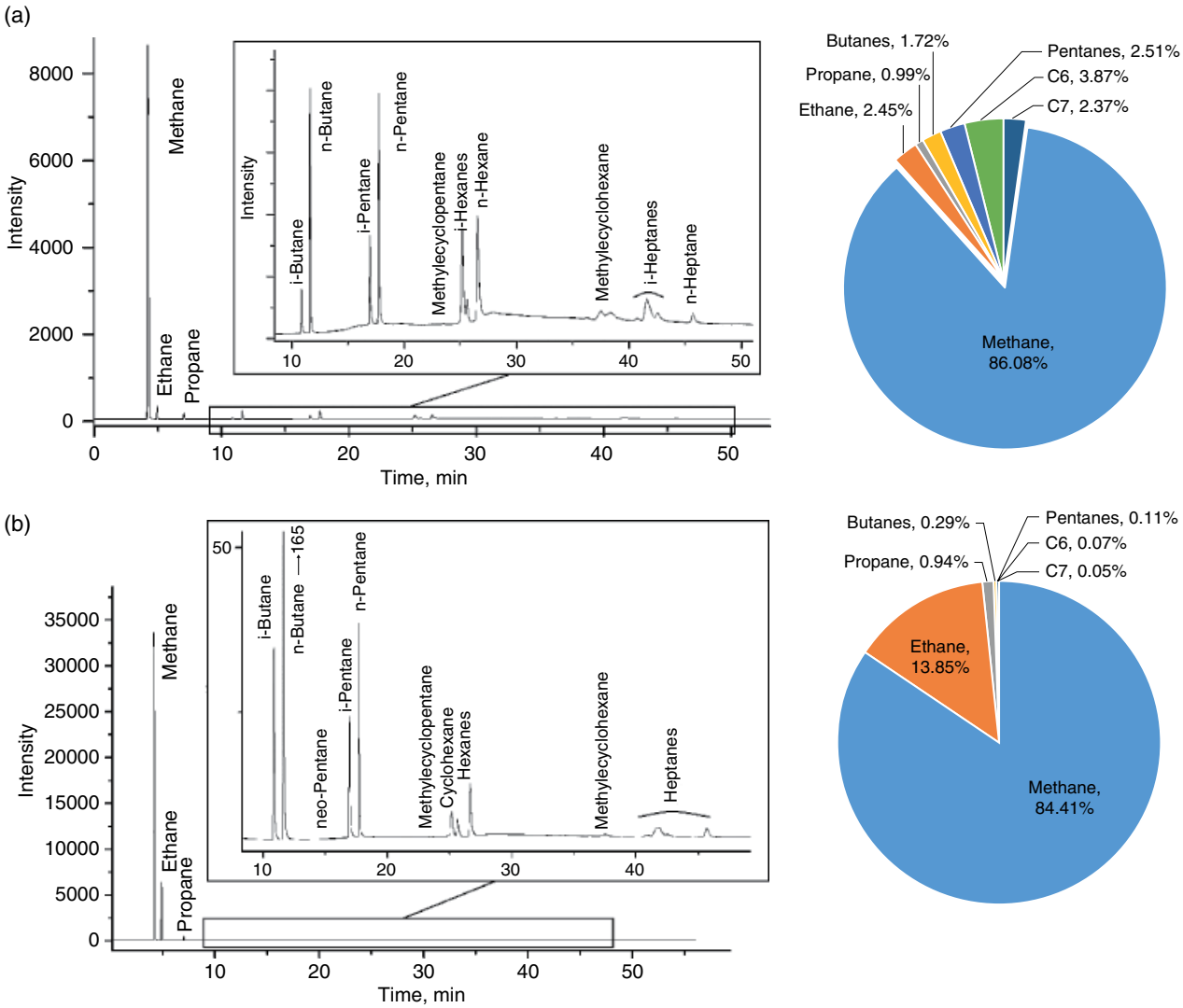

Figure 26.5 The chromatogram (left) and the fraction composition (right) of the hydrocarbon system, formed from the chemical interaction between iron carbide and water at 750 °C and 3.5 GPa (a), and 850 °C and 4.5 GPa (b). See electronic version for color representation of the figures in this book.

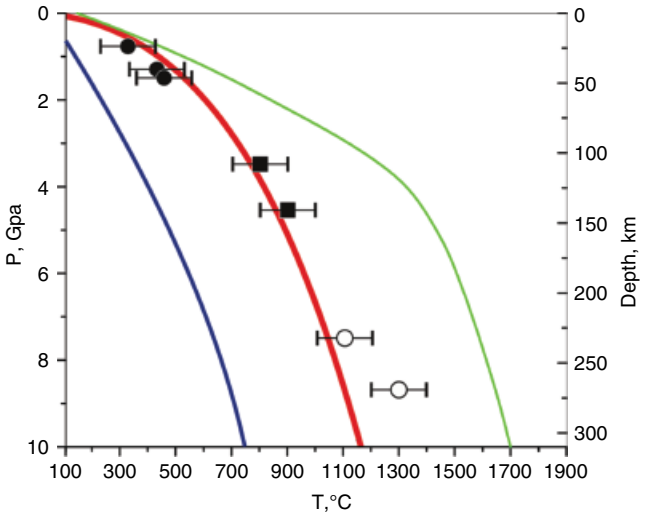

Figure 26.6 Experimental thermobaric conditions. Black circles = experiments with model hydrocarbon system. Open circles = pyroxene-like glass $(Mg_{0.91}Fe_{0.09})(Si_{0.91}Al_{0.09})O_3$ + paraffin oil. Squares = iron oxide (II) $Fe_{0.94}O$ + paraffin oil. Pressure-temperatures profiles of the coldest (blue solid line) and the hottest (red solid line) subducting slabs are taken from Karato (2013). Earth's geotherm (black solid line) is modified after Pollack & Chapman (1977), and the black dashed line is the melting curve of γ-FeH_x (Sakamaki et al., 2009). See electronic version for color representation of the figures in this book.

(and subsequent collision) in the Urals in the Late Paleozoic was oblique and not frontal, accompanied by significant movement of the Ural blocks to the north.

Hydrocarbon data in ultrabasic rocks is especially pertinent alongside experimental results on the behavior of hydrocarbons in the subducted oceanic crust. In the Urals, there are two main types of ultrabasites (S. Ivanov et al., 1975). The first type is alpinotype (ophiolitic), the largest massifs of which are located in the zone of the MUF, extending more than 2,000 km. The second one is platiniferous: area-based dunite-clinopyroxenite-gabbroic massifs located in the suprasubduction zone (K. Ivanov et al., 2007) on the east of the MUF in the Middle and Northern Urals. Different forms of carbon, including bituminous (from traces to 100 g/t), gaseous CO_2, CH_4 forms, and diamonds were found in the ultrabasites of the Urals (Chashchukhin & Votyakov, 2009; Koshkina et al., 1974; Shteinberg & Lagutina, 1984).

The diamonds were found in both types of Ural ultrabasites. Numerous fine diamonds from the ophiolitic massif Rai-Iz of the Polar Urals were studied and described (Yang et al., 2015). There is also a description of the diamond in the dunites of the Kamenushinsky massif of the Platinum Belt of the Urals (Kaminsky, 2007). We believe that the presence of diamonds in ultrabasites indicates their transformation at high pressures at considerable depths in the subduction zone. The intermittent high pressure–low temperature belt of eclogite-glaucophane metamorphic rocks (sometimes containing small diamonds as well) stretches for almost 2000 km in the western part of the MUF. A study of eclogite and glaucophane rocks from the above-mentioned belt show that their formation occurred under pressure of 15 kbar, which corresponds to a depth of 50 km (Lennykh et al., 1995).

The bitumen content found in ultrabasites (serpentinized dunites of different ophiolitic allochthons) is from 1 to 63 g/t. Polycyclic aromatic hydrocarbons, varying from 5 to 103 g/t, were found in these rocks. $C_{14}H_{10}$, $C_{20}H_{12}$, $C_{22}H_{12}$, and $C_{24}H_{12}$ were also identified (Chashchukhin & Votyakov, 2009). The content of heavy alkanes was determined in the ultramafites of the largest alpinotypic massif: Voikar-Synya (Polar Urals): 1.3 g/ton (δ13C = −23.4 ‰) in harzburgite, 1.6 g/ton (δ13C = −26.5 ‰) in wehrlite, 1 g/t in websterite, and 2.3 g/t (δ13C = −26.7 ‰) in pyroxenite. In composition, alkanes in pyroxenite vary from $C_{18}H_{38}$ to $C_{33}N_{68}$ (with a maximum at $C_{22}N_{46}$). They also include pristane ($S_{19}N_{40}$) and phytane ($C_{20}H_{42}$) (Sugisaki & Mimura, 1994). Thus, geological data on the presence of hydrocarbons in ultrabasites squeezed from a slab indicates that complex hydrocarbon systems may exist in a slab at considerable depths. This confirms our experimental results, indicating the stability of hydrocarbons to a depth of 50 km.

Another type of geological observation deals with a result of a study of the primary fluid inclusion in diamonds and garnets, the mantle origin of which is beyond doubt. The composition of the primary fluid inclusion was studied by mass spectrometry in seven native Arkansas diamonds. The result of the investigation has confirmed the presence of different kinds of hydrocarbon in all samples (Melton & Giardini, 1974). Raman and infrared spectroscopy were used to study the composition of the primary fluid in garnet from the Udachnaya kimberlite pipe, (Yakutia, Russia). Primary fluids extracted from garnets comprise saturated hydrocarbons from CH_4 to C_6H_{14} (Tomilenko et al., 2009).

The obtained data on fluid inclusions in natural diamonds and garnets, together with the results of our experiments, have provided conclusive evidence that a mixture of hydrocarbons of similar composition to the main components of natural petroleum can form in the Earth's mantle.

26.5. CONCLUSION

Our experimental results are compatible with the presence of a deep Earth hydrocarbon cycle (Figure 26.7), which can be described as follows.

1. Hydrocarbons accumulated in the traps in the Earth's crust, together with sedimentary rocks immersed in the subducting slab, maintain their stability to a depth of 50 km. The presence of hydrocarbons in ultrabasites

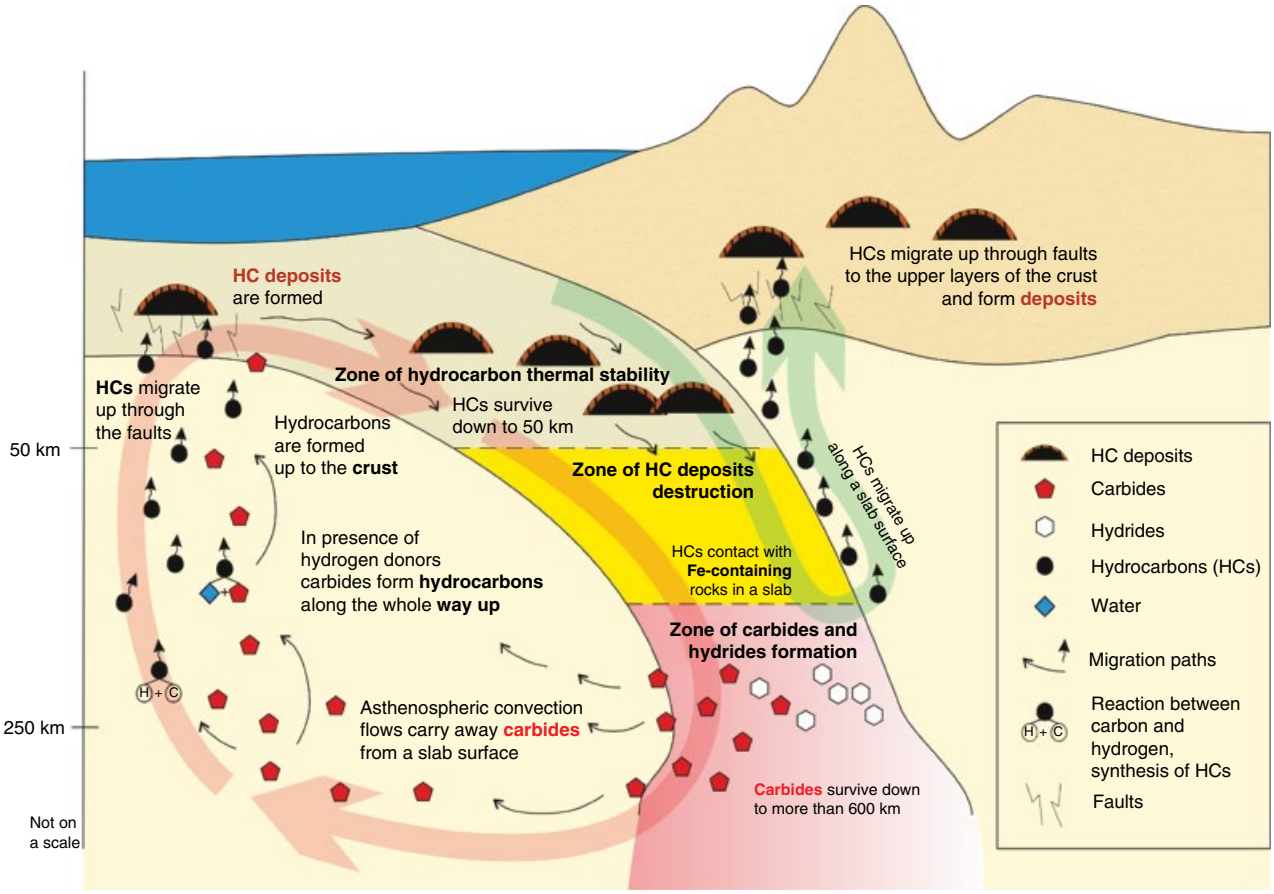

Figure 26.7 Deep hydrocarbon cycle. Hydrocarbons trapped in subducting slabs remain stable at depths of 50 km. At depths of 210–290 km, these hydrocarbons react with surrounding ferrous minerals to form a mixture of iron hydride and iron carbide. This iron carbide transported into the asthenosphere by convective flows reacts with hydrogen or water and form an aqueous hydrocarbon fluid. Water-hydrocarbon mantle fluids can migrate upward through deep faults in the crust, forming multilayer accumulations of oil and gas. Other carbon donors existing in the asthenosphere can also serve as a source of deep hydrocarbons, additional feed for the general upward flow of the water-hydrocarbon fluid. See electronic version for color representation of the figures in this book.

from the Main Uralian Fault, the paleozone of subduction, confirms existence of hydrocarbons in a slab at considerable depths. This observation corresponds with our experimental results and confirms the stability of hydrocarbons to a depth of 50 km.

2. At depths of 50–80 km, the integrity of the traps is disrupted and hydrocarbon fluid enters into contact with surrounding iron-bearing minerals. Lightly saturated hydrocarbons are generated inside the slab from descending carbonates and water.

3. Further immersion transforms the hydrocarbon fluid. At a depth of 80 km, the system consists of hydrocarbon phase, graphite, and water. Methane and other light hydrocarbons can migrate up along the slab–continental plate border.

4. At depths of 210–290 km, light hydrocarbons react with iron-bearing minerals presented in the slab and form a mixture of iron hydride and iron carbide.

5. Iron carbide transported in the asthenosphere by convective flows can react with hydrogen or water present in the asthenosphere and form an aqueous hydrocarbon fluid that can migrate through deep faults into the Earth's upper crust and form multilayer oil and gas deposits in rocks of any lithological composition, genesis, and age.

6. There are other carbon donors in the asthenosphere, in addition to iron carbide coming from the subducting slab. These donors can also serve as a source of deep hydrocarbons. Theoretical calculations (Huang et al., 2017; Karpov et al., 1998; Kenney et al., 2002; Spanu et al., 2011) and experimental results (Kutcherov et al., 2002; Kutcherov et al., 2010; Sokol et al., 2017) show that abiogenic synthesis of complex hydrocarbon systems is possible at temperatures of 900°–1700 °C in the 3–7 GPa pressure range. Similar conditions exist in the layer of the Earth's asthenosphere at depths of 100–250 km. The amount of these hydrocarbons could be significant (Kutcherov et al., 2010).

These hydrocarbons also participate in the deep hydrocarbon cycle, being an additional feed for the general upward flow of the water-hydrocarbon fluid. The presence of hydrocarbons in diamonds and garnets, the mantle origin of which is beyond doubt, corresponds with the above-mentioned theoretical and experimental results and provides evidence that hydrocarbons can form in the Earth's mantle.

ACKNOWLEDGMENTS

V.K., E.M., and A.S. gratefully acknowledge the support of Flotten AB (Sweden) and the Sloan Foundation (USA). K.I. is grateful to RFBR (project 18-05-70016) for its financial support.

REFERENCES

Belonoshko, A. B., Lukinov, T., Rosengren, A., Bryk, T., & Litasov, K. D. (2015). Synthesis of heavy hydrocarbons at the core-mantle boundary. *Scientific Reports*, *5*, 18382.

Bezmen, N. I., Zharikov, V. A., Zevelsky, V. O., & Kalinichev, A. G. (2005). Melting of alkali aluminosilicate systems under hydrogen-water fluid pressure, P_{tot} = 2 kbar. *Petrology*, *13*(5), 407.

Chashchukhin, I. S., & Votyakov, S. L. (2009). Behavior of iron-group elements, oxybarometry, and genesis of unique chromite deposits in the Kempirsai massif. *Geol. Ore Deposits*, *51*(2), 123–138.

Cooper, B. S., Coleman, S. H., Barnard, P. C., & Butterworth, J. S. (1975). Palaeotemperatures in the northern North Sea basin. *Petroleum and the Continental Shelf of North West Europe*, *1*, 487–492.

Dasgupta, R., Mallik, A., Tsuno, K. Withers, A. C., Hirth, G., & Hirschmann, M. M. (2013). Carbon-dioxide-rich silicate melt in the Earth's upper mantle. *Nature*, *493*(7431), 211–222.

Dubrovinsky, L. S., & Saxena, S. K. (1999). Emissivity measurements on some metals and oxides using multiwavelength spectral radiometry. *High Temperatures–High Pressures*, *31*(4), 393–399.

Hessler, A. M., & Sharman, G. R. (2018). Subduction zones and their hydrocarbon systems. *Geosphere*, *14*(5), 2044–2067.

Huang, F., Daniel, I., Cardon, H., Montagnac, G., & Sverjensky, D. A. (2017). Immiscible hydrocarbon fluids in the deep carbon cycle. *Nature Communications*, *8*, 15798.

Ivanov, K. S. (2001). Estimation of paleovelocities of subduction and collision during the formation of the Urals. *Dokl. Earth Sci.*, *377*, 164–167.

Ivanov, K. S., Volchenko, Y., & Koroteev, V. (2007). Nature of the Urals platinum belt and its chromite-platinum metal deposits. *Dokl. Earth Sci.*, *417A*(9), 1304–1307.

Ivanov, S. N., Perfiliev, A. S., Efimov, A. A., Smirnov, G. A., Necheukhin, V. M., & Fershtater, G. B. (1975). Fundamental features in the structure and evolution of the Urals. *Am. J. Sci.*, *275*, 107–130.

Javoy, M. (1997). The major volatile elements of the Earth: Their origin, behavior, and fate. *Geophysical Research Letters*, *24*(2), 177–180.

Kaminsky, F. V. (2007). Non-kimberlitic diamondiferous igneous rocks: 25 years on. *Geological Society of India*, *69*(3), 557.

Kantor, A. P., Jacobsen, S. D., Kantor, I. Y., Dubrovinsky, L. S., McCammon, C. A., Reichmann, H. J., & Goncharenko, I. N. (2004). Pressure-induced magnetization in FeO: Evidence from elasticity and Mössbauer spectroscopy. *Phys. Rev. Lett.*, *93*, 215502.

Karato, S.-I. (2013). *Physics and chemistry of the deep Earth*. Ames, IA: John Wiley & Sons.

Karpov, I. K., Zubkov, V. S., Stepanov, A. N., & Bychinsky, V. A. (1998), Chekaliuk's thermodynamic model of the C-H system: A remake. *Dokl. Earth Sci.*, *358*(1), 30–33.

Kelemen, P. B., & Manning, C. E. (2015). Reevaluating carbon fluxes in subduction zones: What goes down, mostly comes up. *Proceedings of the National Academy of Sciences*, *112*(30), 3997–4006.

Kenney, J. F., Kutcherov, V. A., Bendeliani, N. A., & Alekseev, V. A. (2002). The evolution of multicomponent systems at high pressures: VI. The thermodynamic stability of the hydrogen-carbon system: The genesis of hydrocarbons and the origin of petroleum. *PNAS*, *99*, 10976–10981.

Khurshid, H., Li, W., Chandra, S., Phan, M.-H., Hadjipanayis, G. C., Mukherjee, P., & Srikanth, H. (2013). Mechanism and controlled growth of shape and size variant core/shell FeO/Fe_3O_4 nanoparticles. *Nanoscale*, *5*(17), 7942–7952.

Kolesnikov, A., Kutcherov, V. G., & Goncharov, A. F. (2009). Methane-derived hydrocarbons produced under upper-mantle conditions. *Nature Geoscience*, *2*(8), 566–570.

Kolesnikov, A. Y., Saul, J. M., & Kutcherov, V. G. (2017). Chemistry of hydrocarbons under extreme thermobaric conditions. *ChemistrySelect*, *2*(4), 1336–1352.

Koshkina, T. M., Lagutina, M. V., & Shapiro, V. A. (1974). Cohenite diagnosis in south Urals ultrabasites. *J. Geophys.*, *40*(4), 565–569.

Kumari, R., Krishnia, L., Kumar, V., Singh, S., Singh, H. K., Kotnala, R. K., et al. (2016). Fe_3C-filled carbon nanotubes: Permanent cylindrical nanomagnets possessing exotic magnetic properties. *Nanoscale*, *8*(7), 4299–4310.

Kupenko, I., Dubrovinsky, L., Dmitriev, V., & Dubrovinskaia, N. (2012). In situ Raman spectroscopic study of the pressure induced structural changes in ammonia borane. *J. Chem. Phys.*, *137*(7).

Kutcherov, V. G., Bendeliani, N. A., Alekseev, V. A. & Kenney, J. F. (2002). Synthesis of hydrocarbons from minerals at pressures up to 5 GPa. *Dokl. Phys. Chem.*, *387*, 328–330.

Kutcherov, V. G., Kolesnikov, A. I., Dyugheva, T. I., Kulikova, L. F., Nikolaev, N. N., Sazanova, O. A., & Braghkin, V. V. (2010). Synthesis of complex hydrocarbon systems at temperatures and pressures corresponding to the Earth's upper mantle conditions. *Dokl. Phys. Chem.*, *433*, 132–135.

Lennykh, V. I., Valizer, P. M., Beane, R., Leech, M., & Ernst, W. G. (1995). Petrotectonic evolution of the Maksyutov complex, Southern Urals, Russia: Implications for ultrahigh-pressure metamorphism. *International Geology Review. 37*(7), 584–600.

Mann, P., Gahagan, L., & Gordon, M. B. (2003). Tectonic setting of the world's giant oil and gas fields. In M. T. Halbouty (Ed.), *AAPG memoir* (Vol. *78*, pp. 15–105). AAPG.

Manning, C. E. (2004). The chemistry of subduction-zone fluids. *Earth and Planetary Science Letters*, *223*(1–2), 1–16.

Manning, C. E. (2014). Geochemistry: A piece of the deep carbon puzzle. *Nature Geosci*, *7*(5), 333–334.

Mao, H. K., Xu, J., & Bell, P. M. (1986). Calibration of the ruby pressure gauge to 800 kbar under quasi-hydrostatic conditions. *J. Geophys. Res. B*, *91*, 4673–4676.

Melton, C. E., & Giardini, A. A. (1975). Experimental results and theoretical interpretation of gaseous inclusions found in Arkansas natural diamonds. *Geochim. Cosmochim. Acta*, *60*(56), 413–417.

Mukhina, E., Kolesnikov, A., & Kutcherov, V. (2017). The lower pT limit of deep hydrocarbon synthesis by $CaCO_3$ aqueous reduction. *Scientific Reports*, *7*(1), 5749.

Narygina, O., Dubrovinsky, L. S., McCammon, C. A., Kurnosov, A., Kantor, I. Y., Prakapenka, V. B. & Dubrovinskaia, N. A. (2011). X-ray diffraction and Mössbauer spectroscopy study of fcc iron hydride FeH at high pressures and implications for the composition of the Earth's core. *Earth and Planetary Science Letters*, *307*(3–4), 409–414.

Prescher, C., Dubrovinsky, L., Bykova, E., Kupenki, I., Glazyrin, K., Kantor, A., et al. (2015). High Poisson's ratio of Earth's inner core explained by carbon alloying. *Nature Geosci*, *8*(3), 220–223.

Prescher, C., McCammon, C., & Dubrovinsky, L. (2012). MossA: A program for analyzing energy-domain Mossbauer spectra from conventional and synchrotron sources. *J. Appl. Crystallogr.*, *45*, 329–331.

Sakamaki, K., Takahashi, E., Nakajima, Y., Nishihara, Y., Funakoshi, K., Suzuki, T., & Fukai, Y. (2009). Melting phase relation of FeH_x up to 20 GPa: Implication for the temperature of the Earth's core. *Phys. Earth Planet. Inter.*, *174*(1–4), 192–201.

Shimada, M. (1969). Melting of albite at high pressures in the presence of water. *Earth and Planetary Science Letters*, *6*(6), 447–450.

Shteinberg, D. S., & Lagutina, M. V. (1984). *Carbon in ultrabasites and basites*. Moscow: Nauka.

Sokol, A. G., Tomilenko, A. A., Bul'bak, T. A., & Sobolev, N. V. (2017). Synthesis of hydrocarbons by CO_2 fluid conversion with hydrogen: Experimental modeling at 7.8 GPa and 1350 °C. *Dokl. Earth Sci.*, *477*, 1483–1487.

Sonin, V. M., Bul'bak, T. A., Zhimulev, E. I., Tomilenko, A. A., Chepurov, A. I., & Pokhilenko, N. P. (2014). Synthesis of heavy hydrocarbons under P-T conditions of the Earth's upper mantle. *Dokl. Earth Sci.*, *454*(1), 32–36.

Spanu, L., Donadio, D., Hohl, Schwegler, E., & Galli, G. (2011). Stability of hydrocarbons at deep Earth pressures and temperatures. *Proceedings of the National Academy of Sciences*, *108*(17). 6843–6846.

Sterin, K. E., Aleksanyan, V., & Zhizhin, G. N. (2013). *Raman spectra of hydrocarbons*. Elsevier.

Stern, R. J. (2002). Subduction zones. *Reviews of Geophysics*, *40*(4), 1–38.

Sugisaki, R., & Mimura, K. (1994). Mantle hydrocarbons: Abiotic or biotic? *Geochim. Cosmochim. Acta*, *58*(11), 2527–2542.

Sverjensky, D. A., Stagno, V., & Huang, F. (2014). Important role for organic carbon in subduction-zone fluids in the deep carbon cycle. *Nature Geoscience*, *7*(12), 909–913.

Tao, R., Zhang, L., Tian, M., Zhu, J., Liu, X., Liu, J., et al. (2018). Formation of abiotic hydrocarbon from reduction of carbonate in subduction zones: Constraints from petrological observation and experimental simulation. *Geochim. Cosmochim. Acta*, *239*, 390–408.

Tomilenko, A.A. et al. (2009). Primary hydrocarbon inclusions in garnet of diamondiferous eclogite from the Udachanaya kimberlite pipe, Yakutia. *Doklady Earth Sciences*, *426*(4), 695–698.

Trots, D. M., Kurnosov, A., Ballaran, T. B., Tkachev, S., Zhuravlev, K., Prakapenka, V., et al. (2013). The Sm:YAG primary fluorescence pressure scale. *Journal of Geophysical Research: Solid Earth*, *118*(11), 5805–5813.

Tuinstra, F., & Koenig, J. L. (1970). Raman spectrum of graphite. *The Journal of Chemical Physics*, *53*(3), 1126–1130.

Walrafen, G. E., Abebe, M., Mauer, F. A., Block, S., Piermarini, G. J., & Munro, R. (1982). Raman and X-ray investigations of ice VII to 36.0 GPa. *The Journal of Chemical Physics*, *77*(4), 2166–2174.

Williams, B., Clifford, D., El-Gendy, A. A., & Carpenter, E. E. (2016). Solvothermal synthesis of Fe_7C_3 and Fe_3C nanostructures with phase and morphology control. *Journal of Applied Physics*, *120*(3), 033904.

Yang, J., Robinson, P. T., & Dilek, Y. (2015). Diamond-bearing ophiolites and their geological occurrence. *Episodes*, *38*(4), 344–364.

Zonenshain, L. P., Kuzmin, M. I., & Bocharova, N. Y. (1991). Hot-field tectonics. *Tectonophysics*, *199*(2), 165–192.